Trans-dimensional joint inversion of seabed scattering and reflection data

Gavin Steininger,[a] Jan Dettmer, and Stan E. Dosso
School of Earth and Ocean Sciences, University of Victoria, Victoria, BC V8W 3P6, Canada

Charles W. Holland
Applied Research Laboratory, The Pennsylvania State University, State College, Pennsylvania 16804-0030

(Received 17 October 2012; revised 21 December 2012; accepted 15 January 2013)

This paper examines joint inversion of acoustic scattering and reflection data to resolve seabed interface roughness parameters (spectral strength, exponent, and cutoff) and geoacoustic profiles. Trans-dimensional (trans-D) Bayesian sampling is applied with both the number of sediment layers and the order (zeroth or first) of auto-regressive parameters in the error model treated as unknowns. A prior distribution that allows fluid sediment layers over an elastic basement in a trans-D inversion is derived and implemented. Three cases are considered: Scattering-only inversion, joint scattering and reflection inversion, and joint inversion with the trans-D auto-regressive error model. Including reflection data improves the resolution of scattering and geoacoustic parameters. The trans-D auto-regressive model further improves scattering resolution and correctly differentiates between strongly and weakly correlated residual errors. © *2013 Acoustical Society of America*.
[http://dx.doi.org/10.1121/1.4789930]

PACS number(s): 43.30.Hw, 43.30.Pc, 43.60.Pt, 43.30.Ma [ZHM] Pages: 1347–1357

I. INTRODUCTION

Ocean acoustic reverberation modeling and sonar performance predictions in shallow water require estimates of scattering parameters defining seafloor roughness. Direct measurement of roughness parameters (e.g., stereoscopic photography or laser imaging) is time consuming and expensive. Hence, the estimation of *in situ* seabed roughness from remote acoustic measurements is a problem of practical interest but has received little attention to date. This paper develops a trans-dimensional (trans-D) Bayesian inversion approach to estimate seabed scattering parameters and a layered geoacoustic model, as well as data error parameters, from multi-frequency acoustic scattering and/or reflection data. The approach is applied in simulations based on existing measurement techniques to evaluate the ability of the two data types, inverted separately and jointly, to resolve the seabed parameters.

Simulations represent an important initial step in developing effective measurement/inversion approaches in that the true model is known and may be used to evaluate parameter estimates and uncertainties. Further, error processes can be controlled such that the physics of the acoustic measurements can be examined within specific assumptions (such as lateral homogeneity), without potential complicating factors which may arise in specific experiments. Realistic simulations presented here are based on a geoacoustic test bed located on the Malta Plateau in the Straits of Sicily. In particular, the true geoacoustic profile contains layering at a variety of scales, including fine scales below the resolution of the acoustic data. A flat basement layer (limestone) which supports shear waves is included. Errors include correlations, with both variance and covariance varying with frequency and, for reflection data, with angle.

Bayesian inversion estimates model parameters and uncertainties by quantifying the information content of data and prior, and has been applied widely to geoacoustic inverse problems.[1–7] Bayesian inversion is based on formulating the posterior probability density (PPD) which combines both data information, expressed in terms of a likelihood function, and prior information.[1,8–11] Joint inversion of independent data sets (e.g., scattering and reflection data) is accommodated naturally by formulating a joint likelihood function as the product of the individual likelihoods. An appropriate model parameterization (e.g., number of seabed layers resolved by the data) is generally not known in practice; this is addressed here by trans-D inversion[12,13] which provides an effective automated approach to Bayesian model selection[2,14–17] that has been applied to several problems in geophysics[18–21] and geoacoustics.[22,23] Trans-D inversion samples a set of models (which may vary in dimension) according to the support by the data and prior. In particular, partition modeling and the reversible jump Markov chain Monte Carlo (rjMCMC) algorithm are applied here for trans-D sampling over the number of seabed layers.[22] Including elastic (shear) parameters in the basement makes this layer distinct from the overlying (fluid) sediment layers. Treating layers with different numbers or types of parameters has not been considered previously in trans-D inversion, and requires a novel formulation of the partition prior, which is developed here. Frequency-dependent residual error statistics, including variance and first-order auto-regressive [AR(1)] parameters to model covariance[23,24] of unevenly spaced data, are also sampled (marginalized) in the inversion. The AR(1) coefficients are estimated by trans-D inversion providing an

[a]Author to whom correspondence should be addressed. Electronic mail: gsteinin@uvic.ca

efficient data-driven process to include AR(1) parameters at frequencies where they are required (typically low frequencies) but to omit them where not required to avoid over- or under-parameterizing the error model. The combination of trans-D sampling and hierarchical error modeling provides a rigorous and general inversion approach.

Seabed acoustic scattering data are dependent on both the two-dimensional (2D) seafloor roughness and seabed reflectivity, which is itself dependent on the sub-bottom geoacoustic profile. Since little quantitative work on scattering inversion has been reported, it is of interest to examine to what extent realistic scattering data can resolve roughness parameters and geoacoustic profiles, with resolution characterized here in terms of marginal probability distributions. Possible improvements in parameter resolution in joint scattering/reflection inversion over scattering-only inversion are also of interest. Joint inversion with trans-D error modeling is shown to improve the resolution of scattering parameters, even though the reflection data provide no scattering information, by reducing the uncertainty of geoacoustic parameters.

II. FORWARD MODELS AND DATA

Two forward models are used here to compute mono-static scattering and spherical-wave reflection data, and are applied to a seabed model consisting of a layered half-space as shown in Fig. 1. The top (zeroth) layer is seawater and is assumed to be homogeneous and isotropic with known properties. The seabed is a series of j flat homogeneous layers, terminated by a homogeneous semi-infinite basement ($j+1$ layers with j interfaces in all). Layer properties include interface depth z (the lower boundary of a layer), sound velocity c, density ρ, and attenuation α. As there are $j+1$ layers and only j interfaces, the jth layer does not have an associated interface depth; the depth of the interface between the jth layer and the basement is denoted z_b and considered an attribute of the basement (an important distinction, addressed in Sec. IV). In addition, the basement is assumed to be elastic with a shear-wave velocity c_s and attenuation α_s. The only difference between the seabed model for scattering and reflection is that the water-sediment interface is assumed to be rough for scattering and planar for reflection.

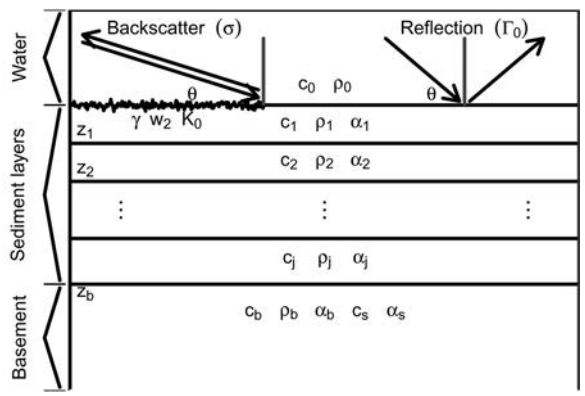

FIG. 1. Schematic diagram of the seabed model. Parameters are defined in the text.

The parameterization and forward models for calculating simulated data are consistent with measurements which have been made at the Malta plateau.[25,26] The geoacoustic parameters of the true model are chosen to represent sand layers over a limestone basement. The layering structure of the true geoacoustic model, shown in Fig. 2, is more complicated than the data can resolve (~100 layers) to allow a meaningful evaluation of the trans-D procedure (Fig. 2 also includes the optimal profile for an inversion discussed later). The true shear-wave velocity and attenuation of the basement are $c_s = 2200$ m/s and $\alpha_s = 0.1$ dB/m/kHz.

In addition to the geoacoustic model it is also necessary to define the residual-error distribution for both scattering and reflection data. The data residuals are assumed to be multivariate Gaussian distributed (as observed for measured reflection-coefficient data[5,22,27]). Residuals at different frequencies are assumed to be independent; however, residuals at the same frequency are not assumed independent over angle.

A. Scattering kernel

The scattering kernel[28] considered here defines the mono-static acoustic backscatter (as a function of angle θ and frequency f) from a single rough interface between two fluid layers (water and first sediment layer) over a layered medium and is given by

$$\sigma'(\theta,f) = \frac{k_0^4 |1+R(\theta,f)|^4}{4} W(2\mathbf{K}) \times \left| 1 - \left(\frac{k_1}{k_0}\right)^2 \frac{\rho_0}{\rho_1} + \left(1 - \frac{\rho_0}{\rho_1}\right) \times \left(\cos^2\theta + \frac{\rho_0}{\rho_1}\sin^2\theta\right) \left(\frac{1-R(\theta,f)}{1+R(\theta,f)}\right)^2 \right|^2, \quad (1)$$

where k_0 and k_1 are the wavenumbers in the water and first sediment layers, and R is the plane-wave reflection coefficient for the $j+1$ layer seabed, which is evaluated recursively and accounts for the elastic basement.[29] In Eq. (1) W

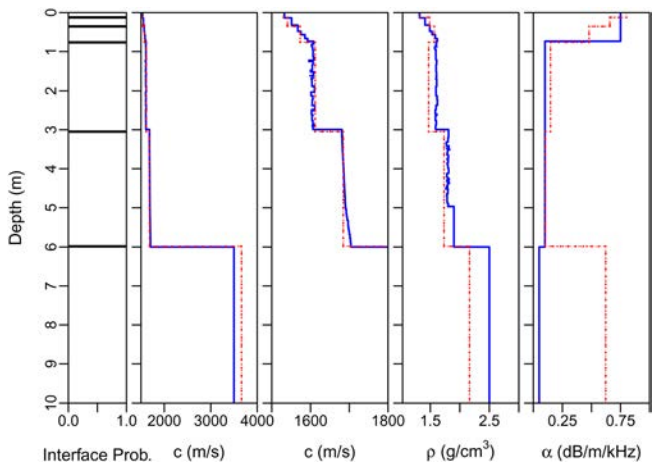

FIG. 2. (Color online) True geoacoustic profile (solid line) and MAP model profile (dotted line) for trans-D auto-regressive inversion (sound velocities shown at two scales).

defines the 2D spatial-roughness power spectrum of the water-sediment interface given by

$$W(\mathbf{K}) = w_2(|\mathbf{K}|^2 + K_0^2)^{-\gamma/2}, \tag{2}$$

where γ, w_2, and K_0 are known as the spectral exponent, spectral strength, and spectral cutoff, respectively, and $\mathbf{K}$ is the transverse component of the wave vector with magnitude $|\mathbf{K}| = k_0 \cos\theta$. Backscatter is considered in decibels

$$\sigma(\theta,f) = 10\log_{10}\sigma'(\theta,f) \ \ (\text{dB}). \tag{3}$$

The scattering errors are assumed to be correlated such that the correlation is non-negative and decreases exponentially with angular separation. To avoid the computational expense of repeatedly taking inverses and determinants of the covariance matrix in the inversion (see Sec. III), the residual correlation structure is modeled using a first-order AR(1) process[23,24,30] given by

$$r_i = a_s^{\Delta\theta_i} r_{i-1} + e_i, \tag{4}$$

where the r_i's are the residuals (indexed over angle), a_s is the AR(1) coefficient, $\Delta\theta_i = \theta_i - \theta_{i-1}$, and e_i are the total residuals, which are identical independently-distributed (IID) Gaussian random variables with zero mean and standard deviation S_s [frequency subscripts in Eq. (4) are omitted for simplicity].

For the simulated data (Fig. 3), the true scattering parameter values are selected to be consistent with measurements:[31] $\gamma = 3.15$, $w_2 = 0.002$, and $K_0 = 1.5$ 1/m. Simulated backscatter data are generated at frequencies of 600 to 3600 Hz and angles of 6° to 19° (the angular range is limited to reduce the effects of sub-surface scatterers). Data errors are Gaussian at each frequency and the AR(1) parameters decrease with frequency (as often observed) such that only errors at 600 and 900 Hz are significantly correlated. The standard deviations and AR(1) parameters of the true model are listed in Table I.

B. Spherical-wave reflection coefficient

Reflection-coefficient data are modeled here using a spherical-wave reflection model to accommodate significant penetration depths.[32] Spherical-wave reflection coefficients $\Gamma_\circ$ for an arbitrary N-layer half-space are computed as a superposition of plane waves (the Sommerfeld integral)[33]

$$\Gamma_\circ(\theta,f) = \frac{ik_0\sqrt{x^2+z^2}}{\exp(ik_0\sqrt{x^2+z^2})} \times \int_0^{\pi/2-i\infty} J_0(k_0 x\cos\theta')\exp(ik_0 z\sin\theta') \times R(\theta',f)\cos\theta'\, d\theta'. \tag{5}$$

In Eq. (5) x and z are the horizontal offset (range) and vertical offset, respectively, and J_0 is the zeroth-order Bessel function. The integral is computed numerically using Simpson's rule.[34] The complex exponential and Bessel function are environment independent, and are pre-computed for an array of argument values.

The covariance structure of the reflection data is similar to that of the scattering data

$$r_i = a_r^{\Delta\theta_i} r_{i-1} + e_i, \tag{6}$$

where the r_i's are the reflection residuals and a_r is the AR(1) parameter. However, in this case the e_i's are not IID in that their assigned standard deviations change at an angle

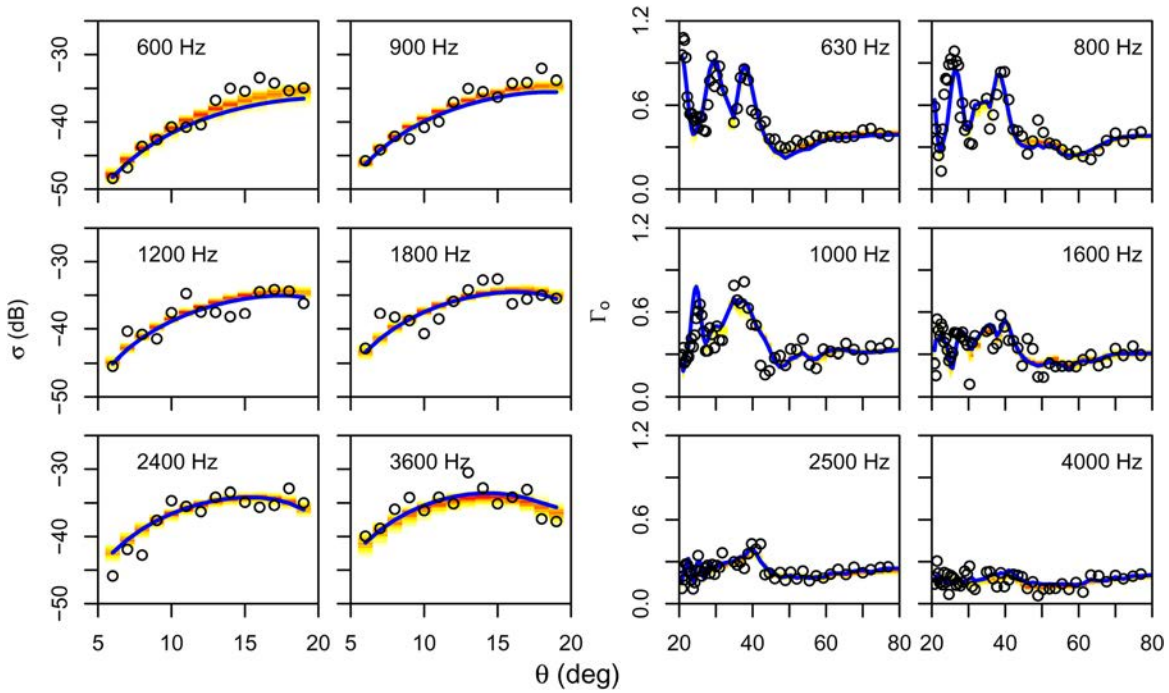

FIG. 3. (Color online) Simulated noisy scattering (left) and reflection-coefficient (right) data (○) and marginal predicted data from joint trans-D auto-regressive inversion (shading). Solid lines indicate noise-free simulated data.

TABLE I. True residual error parameters for scattering (top) and reflection (bottom) data.

Frequency (Hz)	600	900	1200	1800	2400	3600
$\mathbf{S}_s$ (dB)	1.5	1.5	1.5	2.5	1.5	1.5
$\mathbf{a}_s$	0.6	0.5	0.3	0.2	0.1	0
Frequency (Hz)	630	800	1000	1600	2500	4000
$\mathbf{S}_r^L$	0.1	0.1	0.1	0.1	0.05	0.05
$\mathbf{S}_r^H$	0.03	0.03	0.05	0.03	0.03	0.03
$\mathbf{a}_r$	0.7	0.6	0.5	0.2	0.1	0

$\theta_C = 50°$ (approximately the critical angle), since errors commonly change structure at the critical angle. Thus, if $\theta_i < \theta_C$, a low-angle standard deviation S_r^L is used, otherwise a high-angle value S_r^H is used. The data are third-octave band averages from 630 to 4000 Hz with an angular range of 20° to 85° (non-uniformly spaced as obtained in practical measurements[26]). Errors are Gaussian and correlations decrease with frequency (Table I, Fig. 3)

III. BAYESIAN INVERSION

This section provides a brief overview of Bayesian inference as applied to trans-D geoacoustic inversion; for a more complete description of the approach, see Refs. 18, 19, 21, and 22. In Bayesian inversion, model parameters are considered random variables with distributions that evolve, with the addition of data, from the prior distribution to the PPD. Let $\mathbf{d}$ be the vector of N observed data (comprising the scattering and/or reflection measurements at multiple frequencies and angles) and let $\mathcal{J}$ be a countable set (indexed by j) specifying the choice of parameterization (e.g., number of seabed sediment layers), with a set of parameter values denoted $\mathbf{m}_j$ (comprising all unknown roughness, geoacoustic, and error parameters).

Using Bayes' rule the trans-D PPD can be written as[12]

$$P(j,\mathbf{m}_j|\mathbf{d}) = \frac{\pi(\mathbf{m}_j)\mathcal{L}(\mathbf{m}_j)}{\mathcal{Z}} = \frac{P(j)P(\mathbf{m}_j|j)P(\mathbf{d}|j,\mathbf{m}_j)}{\sum_{j'\in\mathcal{J}}\int P(j')P(\mathbf{m}'_{j'}|j')d\mathbf{m}'_{j'}P(\mathbf{d}|j',\mathbf{m}'_{j'})d\mathbf{m}'_{j'}}, \quad (7)$$

where $\pi(\mathbf{m}_j) = P(j)P(\mathbf{m}_j|j)$ is the prior distribution of j and $\mathbf{m}_j$, $\mathcal{L}(\mathbf{m}_j) = P(\mathbf{d}|j,\mathbf{m}_j)$ is the likelihood of the parameter vector [$P(\mathbf{d}|j,\mathbf{m}_j)$ interpreted as a function of $\mathbf{m}_j$ for a fixed $\mathbf{d}$], and $\mathcal{Z}$ is the total evidence of the ensemble of models. Here the data residuals are assumed to be Gaussian distributed, leading to the likelihood function

$$\mathcal{L}(\mathbf{m}_j) = \frac{1}{(2\pi)^{N/2}|\mathbf{C}_d|^{1/2}}\exp\left(-\frac{1}{2}[\mathbf{d}-\mathbf{d}(\mathbf{m}_j)-\mathbf{d}(\mathbf{a})]^{\top} \times \mathbf{C}_d^{-1}[\mathbf{d}-\mathbf{d}(\mathbf{m}_j)-\mathbf{d}(\mathbf{a})]\right), \quad (8)$$

where $\mathbf{C}_d$ is a diagonal covariance matrix with ith diagonal element equal to the variance of the ith total residual [e_i from Eqs. (4) and (6) for scattering and reflection data, respectively].[24] In Eq. (8) the vector $\mathbf{d}(\mathbf{m}_j)$ represents the data predicted by the forward models [Eqs. (3) and (5) for scattering and reflection data, respectively] for parameters $\mathbf{m}_j$. The vector $\mathbf{d}(\mathbf{a})$ represents the AR(1) process; i.e., for a given data type and frequency $d_i(\mathbf{a}) = a^{\Delta\theta_i} r_{i-1}$ $(\mathbf{m}_j)$, where $\mathbf{r}(\mathbf{m}_j) = \mathbf{d} - \mathbf{d}(\mathbf{m}_j)$.

The trans-D PPD is sampled using the rjMCMC algorithm, which creates a Markov chain that converges to the PPD.[9] Let $\mathbf{m}_j$ be the current Markov chain state and $Q(\mathbf{m}'_{j'}|\mathbf{m}_j)$ be the proposal distribution by which a new state $\mathbf{m}'_{j'}$ is generated. The proposed model can represent a perturbation of the parameters of $\mathbf{m}_j$ or a change (jump) in dimension of $\mathbf{m}_j$, i.e., $j' \neq j$. The proposed state $\mathbf{m}'_{j'}$ is accepted with probability

$$A = \min\left[1, \frac{\pi(\mathbf{m}'_{j'})\mathcal{L}(\mathbf{m}'_{j'})Q(\mathbf{m}_j|\mathbf{m}'_{j'})}{\pi(\mathbf{m}_j)\mathcal{L}(\mathbf{m}_j)Q(\mathbf{m}'_{j'}|\mathbf{m}_j)}|\mathrm{J}|\right], \quad (9)$$

where $\mathbf{J}$ is the Jacobian of the diffeomorphism between the parameter spaces associated with $\mathbf{m}_j$ and $\mathbf{m}'_{j'}$. For the common case of fixed-dimensional (fixed-D) inversion with uniform prior and symmetric proposal, Eq. (9) simplifies to the likelihood ratio

$$A = \min\left[1, \frac{\mathcal{L}(\mathbf{m}'_{j'})}{\mathcal{L}(\mathbf{m}_j)}\right]. \quad (10)$$

IV. PRIOR INFORMATION

In denoting the parameterization of a model as $\mathbf{m}_j$, the subscript indicates that the number of parameters of the model depends on j, the number of sediment layers. The model vector is a list of parameter vectors, $\mathbf{m}_j = (j, \mathbf{z}_j, \boldsymbol{\beta}, \boldsymbol{\Sigma}, \boldsymbol{\chi}_j, \mathbf{S}_s, \mathbf{S}_r, \mathbf{a}_s, \mathbf{a}_r)$, where $\mathbf{z}_j$ represents the sediment partition; $\boldsymbol{\beta}$ represents the basement parameters c_b, α_b, c_s, α_s, and ρ_b; $\boldsymbol{\Sigma}$ represents the scattering parameters γ, w_2, and K_0; $\boldsymbol{\chi}_j$ contains the three vectors of sediment parameters $\mathbf{c}_j$, $\boldsymbol{\rho}_j$, and $\boldsymbol{\alpha}_j$; $\mathbf{S}_s$ and $\mathbf{S}_r = (\mathbf{S}_r^L, \mathbf{S}_r^H)$ contain the standard deviations for scattering and reflection-coefficient data, respectively; and $\mathbf{a}_s$ and $\mathbf{a}_r$ contain the AR(1) parameters for scattering and reflection data.

The prior distribution $P(\mathbf{m}_j)$ can be written as a hierarchical distribution $P(\mathbf{m}_j) = P(\mathbf{z}_j|j,\boldsymbol{\beta})P(\chi_j|j)P(\boldsymbol{\Sigma})P(\boldsymbol{\beta})P(j)P(\mathbf{S}_s) \times P(\mathbf{S}_r)P(\mathbf{a}_s)P(\mathbf{a}_r)$. The independent distributions are assumed to be uniform over some interval of width $\Delta* = *_U - *_L$ (* represents an arbitrary parameter); the upper and lower parameter limits used here are given in Table II. The conditional prior distribution for the physical parameters of the sediment layers is thus $P(\chi_j|j) = (\Delta c \Delta\alpha \Delta\rho)^{-j}$ when the parameters are within the prior bound and zero otherwise. A collection of laboratory and *in situ* measurements[35,36] is used to create joint priors for ρ and c for both the sediment and basement layers, as shown in Fig. 4.

The interpretation of the conditional prior distribution for the partition $P(\mathbf{z}_j|j,\boldsymbol{\beta})$ is more complicated and requires a novel formulation developed here. Let $\mathbf{z}'_j = \mathbf{z}_j/z_b$, then $P(\mathbf{z}'_j|j,\boldsymbol{\beta})$ is assumed to be a Dirichlet distribution, $P(\mathbf{z}'_j|j,\boldsymbol{\beta}) = \mathrm{Dir}(\mathbf{z}'_j|p_1,p_2,\ldots,p_j)$, where $p_1,\ldots,p_j$ are the Dirichlet parameters. The Dirichlet distribution is a generalization of the binomial distribution that describes the probability of the

TABLE II. Lower and upper prior bounds (LB and UB) for basement, sediment, and scattering parameters.

Basement			Sediment		
Parameter	LB	UB	Parameter	LB	UB
z_b (m)	0	10	c (m/s)	1450	2100
ρ_b (g/cm^3)	1.20	3.00	α (dB/m/kHz)	0	1
c_b (m/s)	1500	6000	ρ (g/cm^3)	1.20	2.25
α_b (dB/m/kHz)	0	1	Scattering		
c_s (m/s)	0	$c_b/\sqrt{2}$	Parameter	LB	UB
α_s (dB/m/kHz)	0	1	γ	2	4
			w_2	10^{-5}	10
			K_0 (1/m)	10^{-5}	32

partition of one unit into j parts.[8] The distribution $P(\mathbf{z}_j|j, \boldsymbol{\beta})$ is found by making a variable transform of $\mathbf{z}'_j$ to $\mathbf{z}_j$. In addition, it is assumed that all possible partitions are equally probable, which is equivalent to assuming that all Dirichlet parameters are unity. Thus $P(\mathbf{z}_j|j, \boldsymbol{\beta}) = (j-1)!z_b^{-(j-1)}$.

In other partition inversion work[9,19,20,22] an alternative method of describing the prior, referred to as the "grid trick," is used. The grid trick assumes a discrete set of possible partition locations corresponding to an underlying grid, such that $P(\mathbf{z}_l|l) = (l!(G-l)!)/G!$, where G is the number of grid points and l is the number of layers (because the interface depth of the basement is interpreted differently in the two methods the definition of the number of layers is also different, $l = j-1$). It is then found that the number of grid points cancels out in the acceptance probability, Eq. (9), and consequently an explicit value for G is not required. However the grid trick cannot be used here since the elastic basement is distinct from overlying fluid layers. The Dirichlet prior developed above precludes the need for a fictitious grid, and even if the maximum depth of the partition is known, it has the advantage that it allows for the prior (and consequently the posterior) probability of a model to be evaluated explicitly (not normally possible with the grid trick). This is advantageous in application which require selecting a "best" (i.e., most-probable) model.

V. SAMPLING SCHEME

In trans-D inversion, the proposal distribution Q randomly selects between three types of moves at each step: Perturb, Q_P; birth, Q_B; and death, Q_D. If Q_P is selected, all parameters in the model are updated. If Q_B is selected, an interface is proposed at a random depth, and the geoacoustic parameters of the proposed layer are defined by perturbing the previous values at that depth. Finally, if Q_D is selected, a randomly-chosen sediment layer is removed. The acceptance probability, Eq. (9), can thus be rewritten as

$$A = \min\left[1, \frac{\pi(\mathbf{m}'_{j'})}{\pi(\mathbf{m}_j)}\frac{\mathcal{L}(\mathbf{m}'_{j'})}{\mathcal{L}(\mathbf{m}_j)} \times \frac{Q_P(\mathbf{m}_j|\mathbf{m}'_{j'}) + Q_B(\mathbf{m}_j|\mathbf{m}'_{j'}) + Q_D(\mathbf{m}_j|\mathbf{m}'_{j'})}{Q_P(\mathbf{m}'_{j'}|\mathbf{m}_j) + Q_B(\mathbf{m}'_{j'}|\mathbf{m}_j) + Q_D(\mathbf{m}'_{j'}|\mathbf{m}_j)}\right]. \quad (11)$$

Consider first the perturbation step. Here all parameters are updated sequentially using a symmetric proposal distribution so the proposal ratio is unity. Since the prior distribution of interface depths for any $\mathbf{m}_j$ is not uniform, even given j, the priors do not generally cancel, and the prior ratio must be evaluated. The prior ratio for a perturbation move is

$$\left(\frac{\pi(\mathbf{m}'_{j'})}{\pi(\mathbf{m}_j)}\right)_P = \left(\frac{z_b}{z'_b}\right)^{(j-1)}, \quad (12)$$

and the acceptance probability for a perturbation step can be written as

$$A_P = \min\left[1, \left(\frac{z_b}{z'_b}\right)^{(j-1)}\frac{\mathcal{L}(\mathbf{m}'_j)}{\mathcal{L}(\mathbf{m}_j)}\right]. \quad (13)$$

Both the prior and proposal ratios for the birth step do not cancel and must be evaluated. The prior ratio for the birth step is

$$\left(\frac{\pi(\mathbf{m}'_{j'})}{\pi(\mathbf{m}_j)}\right)_B = \left(\frac{H_c}{\Delta c\Delta\alpha\Delta\rho}\frac{j}{z_b}\right), \quad (14)$$

where H_c is the product of the uniform priors for ρ and c divided by the total area of their joint prior. The proposal ratio for the birth step is

$$\left(\frac{Q_D(\mathbf{m}_j|\mathbf{m}'_{j'})}{Q_B(\mathbf{m}'_{j'}|\mathbf{m}_j)}\right)_B = \frac{z_b}{j}Q_n(\chi'|\chi), \quad (15)$$

where χ' and χ are vectors of geoacoustic parameters for the new layer and the previous values at the depth of the proposed interface, and here Q_n is a multi-variate Gaussian distribution centered at χ. The acceptance probability for the birth step is

$$A_B = \min\left[1, \frac{H_c}{\Delta c\Delta\alpha\Delta\rho}\frac{1}{Q_n(\chi'|\chi)}\frac{\mathcal{L}(\mathbf{m}'_{j'})}{\mathcal{L}(\mathbf{m}_j)}\right]. \quad (16)$$

The acceptance probability of the death step can be found in a similar way to be

$$A_D = \min\left[1, \frac{(\Delta c\Delta\alpha\Delta\rho)}{H_c}Q_n(\chi'|\chi)\frac{\mathcal{L}(\mathbf{m}'_{j'})}{\mathcal{L}(\mathbf{m}_j)}\right]. \quad (17)$$

In addition to inverting for the geoacoustic parameters trans-dimensionally the same framework can be applied to

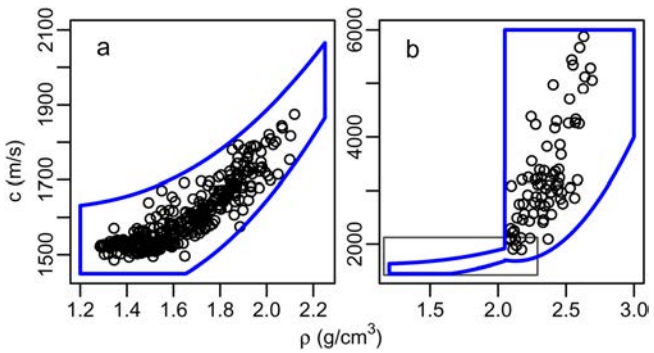

FIG. 4. (Color online) Joint prior bounds for c and ρ for (a) sediments and (b) basement. Empirical (Refs. 35 and 36) data are plotted as circles. The gray rectangle in (b) shows the extent of the sediment prior in the basement.

the AR(1) parameters such that the parameters can be added or removed to avoid over- or under-parameterizing the error model. There are again three moves: Birth, death, and perturbation, with acceptance probabilities (a_B, a_D, and a_P) and proposal distributions (q_B, q_D, and q_P), respectively. To describe the trans-D AR(1) procedure, consider a case with only one AR(1) parameter and a fixed number of other model parameters. The model subscript is taken to refer to the status of the AR(1) parameter with $\mathbf{m}_0$ representing a model without the AR(1) and $\mathbf{m}_1$ representing a model with the AR(1) parameter. A model without the AR(1) parameter always proposes a birth and the new value is sampled from the prior distribution, $q_B = p(\mathbf{m}_1'|\mathbf{m}_0) = \Delta a^{-1}$. Conversely, a model with the AR(1) parameter randomly proposes a death or perturbation move: $q_D = p(\mathbf{m}_0'|\mathbf{m}_1) = 0.5$ and $q_P = 0.5\,\tilde{q}_P(\mathbf{m}_1'|\mathbf{m}_1)$, where $\tilde{q}_P$ is a Gaussian proposal distribution centered at the current AR(1) value. Using these definitions the acceptance probability for birth, death, and perturbation moves, respectively, are

$$a_B = \min\left[1, \frac{1}{2}\frac{\mathcal{L}(\mathbf{m}_1')}{\mathcal{L}(\mathbf{m}_0)}\right], \tag{18}$$

$$a_D = \min\left[1, 2\frac{\mathcal{L}(\mathbf{m}_0')}{\mathcal{L}(\mathbf{m}_1)}\right], \tag{19}$$

$$a_P = \min\left[1, \frac{\mathcal{L}(\mathbf{m}_1')}{\mathcal{L}(\mathbf{m}_1)}\right]. \tag{20}$$

The convergence of rjMCMC algorithms can be slow. To improve mixing (speed of convergence), population methods can be used. These are based on drawing samples from the product of multiple distributions, at least one of which is the PPD.[23,37] Markov chains are allowed not only to wander within a given distribution but also to interchange (swap) with chains in other distributions.

The choice of additional distributions used here is

$$P_T(\mathbf{m}_j) = \frac{\pi(\mathbf{m}_j)\mathcal{L}(\mathbf{m}_j)^{1/T}}{\sum_{j'\in\mathcal{J}}\int_{\mathcal{M}}\pi(\mathbf{m}_{j'}')\mathcal{L}(\mathbf{m}_{j'}')^{1/T}d\mathbf{m}_{j'}'}, \tag{21}$$

where T is known as the sampling temperature. Population-based sampling using this collection of distributions is called parallel tempering.[38,39] Equation (21) can be interpreted as the standard PPD with the likelihood raised to the power $1/T$. If $T > 1$ the significance of the data relative to the prior is diminished; if $T < 1$ the significance of the data is exaggerated. Models selected from distributions with $T > 1$ tend to under-fit the data and have j values lower than those for models sampled from the PPD; models sampled from distributions with $T < 1$ tend to over-fit the data and have higher j values.

The acceptance probability for a parallel tempering swap move is[37]

$$A_S = \min\left[1, \left(\frac{\mathcal{L}(\mathbf{m}_{j'}')}{\mathcal{L}(\mathbf{m}_j)}\right)^{(1/T-1/T')}\right]. \tag{22}$$

Equation (22) assumes that swapping partners are selected such that the probability of one chain picking another chain as its partner is the same as the reverse; if this condition is met, any system for selecting partners is allowed. Inversions in this paper were run in parallel on 31 groups each consisting of 10 Markov chains. Only Markov chains within the same group interact. Each group had one chain with $T = 1$, two chains with $T < 1$, and seven chains with $T > 1$. The T values form a geometric progression $T_{i+1}/T_i = 1.175$.

VI. INVERSION RESULTS

Three inversions of the simulated data are considered here. The first uses only the scattering data, the second uses both scattering and reflection data, and the third uses both data sets with trans-D sampling of the AR(1) parameters. These inversions are referred to as scattering-only, joint, and joint trans-dimensional auto-regressive (TDAR), respectively. In each case, approximately 2 000 000 samples were collected at $T = 1$ and ~400 000 samples from the start of the chains were deleted (burn-in). The remaining samples were chain thinned by a factor of 8 to reduce the autocorrelation.

A. PPD

The marginal posterior distributions of the scattering parameters for the three inversions are shown in Fig. 5. The marginals for the scattering-only inversion for γ and K_0 are not well determined within their prior bounds; the data are unable to differentiate γ from the prior bound of 4 or K_0 from 0. The joint inversion improves the resolution of γ; the marginal now has a clear mode centered near the true value. However, the joint inversion appears to slightly degrade the resolution of w_2. The TDAR inversion further improves the resolution of γ. Table III gives the standard deviation about the true solution for scattering parameters; the TDAR inversion provides the highest accuracy for all parameters.

Figures 6 and 7 show the marginal profiles for geoacoustic parameters from scattering-only and TDAR inversions, respectively (the joint-inversion profile is indistinguishable

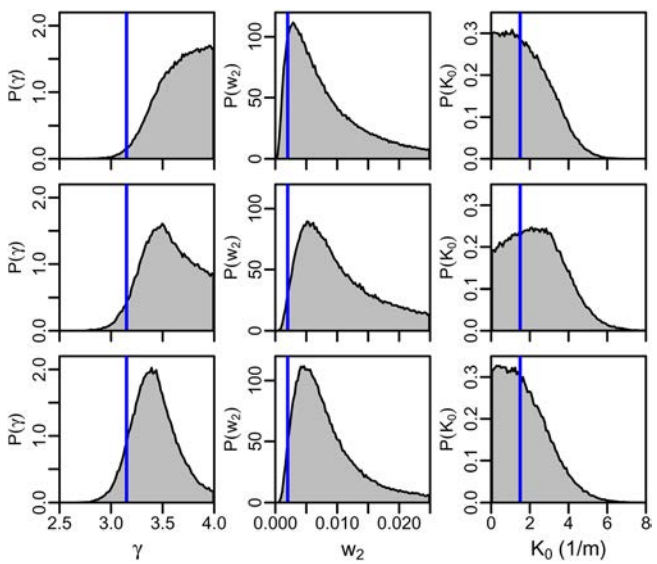

FIG. 5. (Color online) Marginal posterior distributions of the scattering parameters for top: Scattering-only inversion; middle: Joint inversion; bottom: Joint TDAR inversion. Vertical lines indicate the true values.

TABLE III. Standard deviation about true values for scattering parameters.

Inversion	γ	w_2	K_0 (1/m)
Scattering-only	0.562	0.0139	1.278
Joint	0.465	0.0188	1.655
TDAR	0.342	0.0120	1.277

from the TDAR profile). For the scattering-only inversion, the near-surface velocity and density values are well determined and there is an indication of the positive gradient over the top ~1 m. Below 3 -m depth the scattering data are unable to resolve any structure. High attenuation is indicated to 0.5 m depth; below this there is essentially no information.

The joint inversions (Fig. 7) have much smaller posterior uncertainty than the scattering-only inversion, particularly at depth. The joint inversions resolve c and ρ for the entire profile depth; α is resolved to the depth of the basement (6 m). In particular, the joint inversions follow the gradient in c from 0 to 0.9 m, and find the discontinuities at 3 and 6 m. Velocity uncertainties are small (relative to their prior bounds). The density and attenuation profiles agree well with the true model but have larger uncertainties than the velocity profile. The joint inversions resolve the basement interface depth but not the slight gradient in c from 5 to 6 m depth.

The marginal posterior distributions of the basement parameters for the joint TDAR inversion are shown in Fig. 8 (scattering-only inversion results are not shown as parameters are unresolved). The shear-wave velocity is well determined (marginal width ~75 m/s) with significant probability at the true value. The compressional-wave velocity is less well determined (marginal width ~800 m/s) but does also have significant probability at the true value. Since high c_b and c_s values are resolved, the data clearly identify the basement as limestone rather than sediment. The better resolution of c_s than c_b results from the smaller contrast between the sediment sound velocity (c_j) and c_s than between c_j and c_b. In cases where the ratio between c_j and c_s is greater than

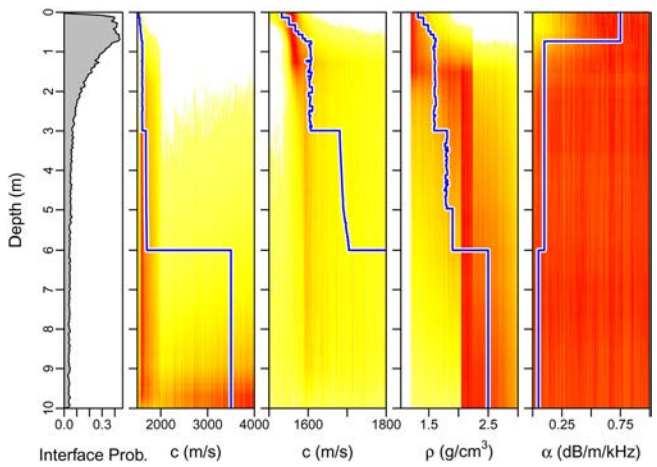

FIG. 6. (Color online) Marginal posterior geoacoustic profiles from scattering-only inversion (sound velocities shown at two scales). Solid lines indicate true profiles. Probability values are normalized independently for each depth for display purposes.

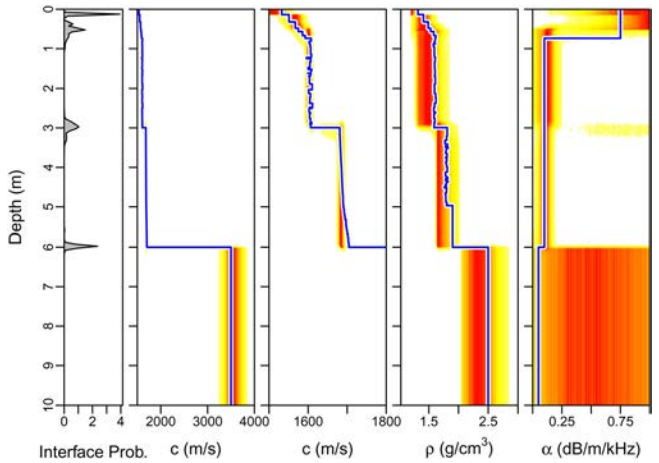

FIG. 7. (Color online) Marginal posterior geoacoustic profiles from joint TDAR inversion (joint inversion results are essentially identical). Solid lines indicate true profiles. Probability values are normalized independently for each depth for display purposes.

between c_j and c_b, c_b is observed to be better resolved than c_s.[11] An inversion that treated the basement as fluid, rather than an elastic solid, strongly biased the compressional-wave velocity and density estimates (not shown).

The results so far are presented in terms of posterior marginal distributions; however, some applications may require an estimate of the optimal model. Here the maximum *a posteriori* (MAP) model is used. This also highlights the significance of being able to explicitly evaluate the prior distribution as such an estimate is not possible otherwise. The MAP geoacoustic profile for the TDAR inversion is given in

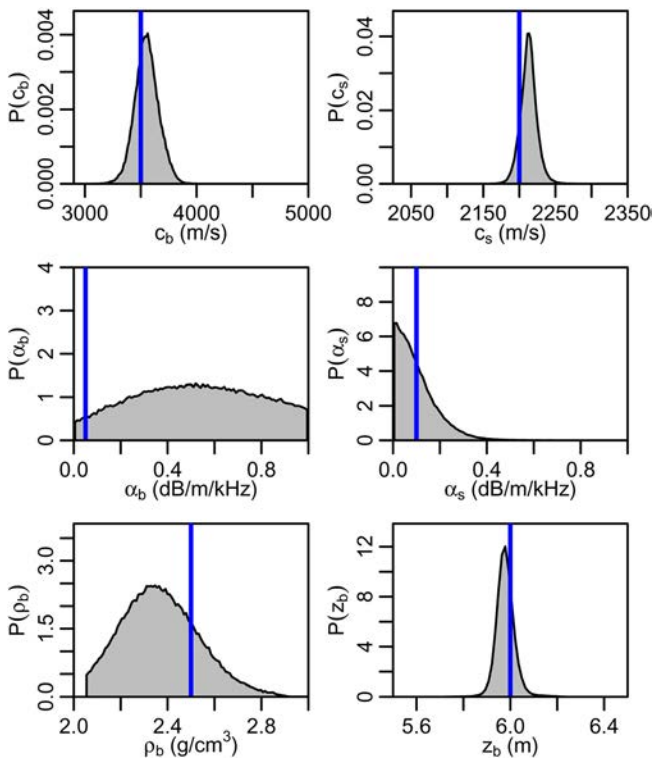

FIG. 8. (Color online) Marginal posterior distributions of basement geoacoustic parameters from joint TDAR inversion. Vertical lines indicate true values.

TABLE IV. The scattering and geoacoustic parameter values of $\hat{\mathbf{m}}_j$, the model with maximum posterior probability for the TDAR inversion.

Sediment			
z (m)	c (m/s)	ρ (g/cm^3)	α (dB/m/kHz)
0.124	1530	1.330	0.8002
0.355	1540	1.488	0.6573
0.764	1573	1.568	0.4793
3.048	1612	1.472	0.1473
	1684	1.733	0.1026
Basement		Scattering	
z_b (m)	5.984	γ	3.126
c_b (m/s)	3662	w_2	0.0017
c_s (m/s)	2209	K_0 (1/m)	1.507
ρ (g/cm^3)	2.165		
α_b (dB/m/kHz)	0.6218		
α_s (dB/m/kHz)	0.0296		

Fig. 2; all seabed parameters are given in Table IV. The MAP scattering parameters are close to their true values. Figure 2 shows that the MAP seabed sound-speed profile closely follows the true model, although with less structure (fewer layers) than the true model. The MAP density and attenuation profiles are generally good representations over the sediment layers but differ more from the true model in the basement (where the marginal probability profiles in Fig. 7 indicates larger uncertainties). The MAP model has interfaces very close to both of the large discontinuities in the true profile.

B. Data-fit

The fit to the scattering data is shown in terms of marginal predicted data in Fig. 9 for the scattering-only inversion and Fig. 3 for the TDAR inversion. These figures also show the observed (noisy) data which were inverted and the noise-free data. The agreement between predicted and noise-free data is good. The introduction of the reflection data reduces the variance of the predicted data about the noise-free data at all frequencies. In addition, the TDAR inversion further reduces the variance at high frequencies. These comparisons are, of course, not possible in practical cases when the noise-free data are unknown. In such cases it is natural to consider the data residuals.

The standardized total residuals ($\hat{\mathbf{e}}$) are defined as the total residuals divided by their standard deviations; i.e.,

$$\hat{e}_i = \frac{e_i}{S_i} = \frac{d_i - d_i(\mathbf{m}_j) - d_i(\mathbf{a})}{S_i}, \tag{23}$$

where the data type and frequency subscripts are omitted for clarity. The standardized total residuals for the scattering and reflection data for the TDAR inversion are shown in Fig. 10. The scattering residuals appear stationary, uncorrelated, and unbiased. The residuals for the reflection data also appear homostochastic although there appears to be some residual structure at 630 and 1000 Hz. This is not unexpected as the true geoacoustic profile was selected so it could not be fully resolved by the inversion. Such theory error (the true model is not in the parameter space of the inversion) commonly results in correlated residuals.[16,17,24]

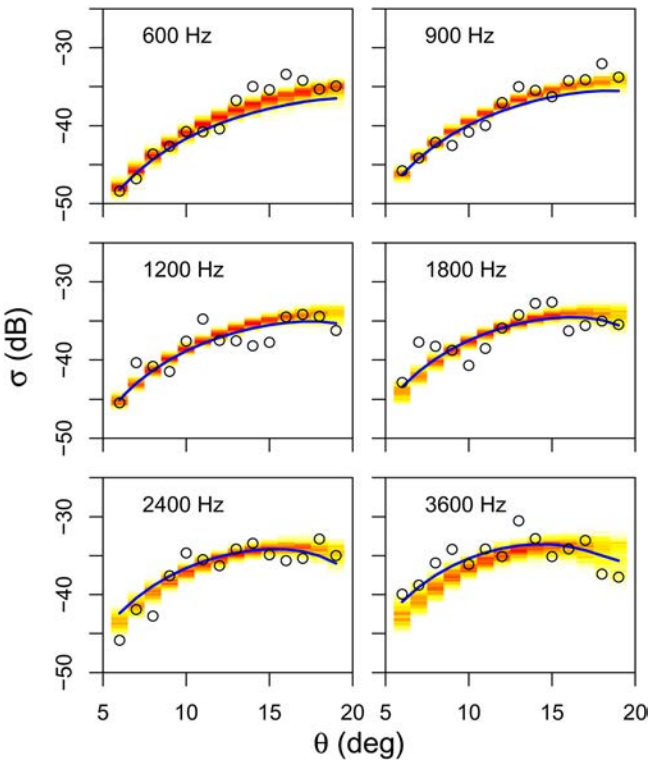

FIG. 9. (Color online) Simulated noisy scattering data (°) and marginal predicted data (shading) from scattering-only inversion. Solid lines indicate noise-free simulated data.

Figures 11 and 12 show the marginal distributions for the residual standard deviation and AR(1) parameters from the joint inversion. To evaluate whether residuals with significant correlations were correctly identified by the joint inversion, a location test is applied to all AR(1) parameters.[24] The true distributions of the posterior means of the AR(1) parameters under the null hypotheses (H_0: $\mathbf{a_s} = \mathbf{a_r} = \mathbf{0}$) are not known analytically; however, they can be approximated using Monte Carlo simulation. This simulation consists of drawing sets of uncorrelated Gaussian random variables and inverting for the AR(1) model [Eq. (4) or (6)]. The distribution (over many random draws) of the sampled means is used as the null distribution. The location tests quantifies evidence (in terms of a p value) against the null hypothesis H_0 that the AR(1) sample means are drawn from the null distribution. The results of the location tests are given in Table V. A p value >0.05 is interpreted as no significant evidence against H_0, i.e., no evidence the residuals are serially correlated. A p value <0.05 is interpreted as significant evidence against H_0, indicating the residuals are correlated. The inversion procedure correctly identifies the strongly correlated residuals (a_s, $a_r \geq 0.5$) from the weakly correlated ones (a_s, $a_r \leq 0.1$). Moderately-correlated residuals ($0.2 \leq a_s, a_r \leq 0.3$) are not identified.

Generally, AR(1) parameters found to be insignificant could be excluded to avoid over-parameterizing the error model and the inversion repeated. However, this approach is not entirely satisfactory as removing AR(1) parameters is equivalent to fixing their value at zero, and there is insufficient

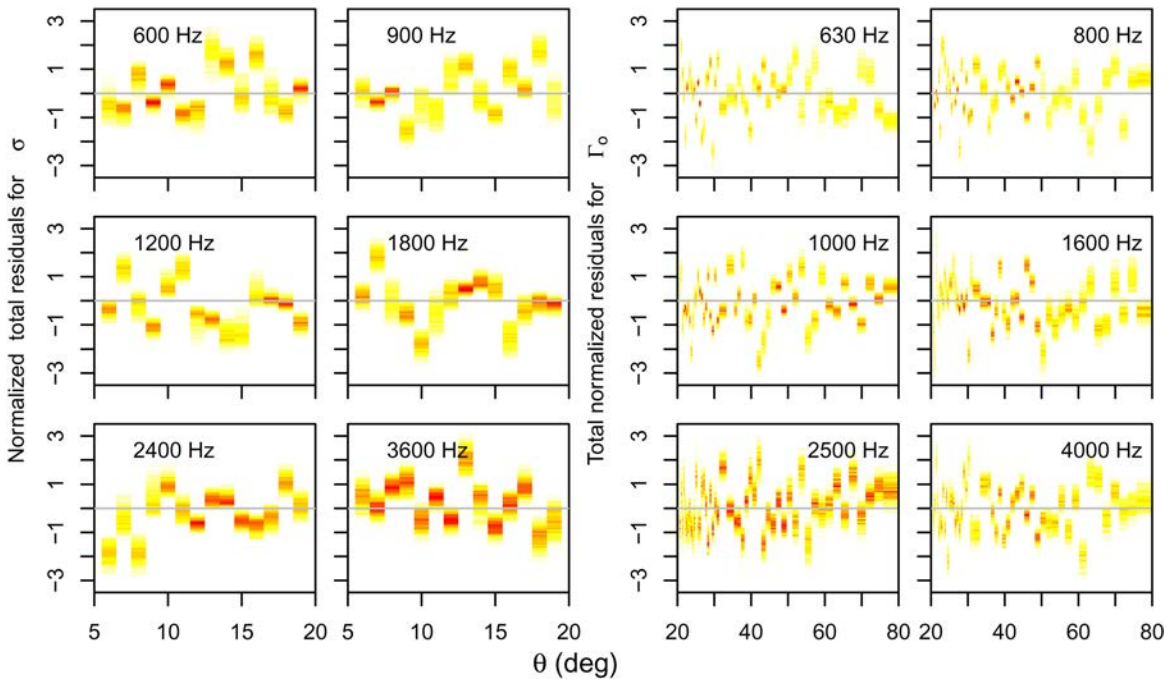

FIG. 10. (Color online) Marginal standardized total residuals, $\hat{e}$, from joint TDAR inversion of scattering data (left) and reflection-coefficient data (right).

evidence to make such a strong assumption. The TDAR inversion samples AR(1) parameters according to their support by the data and scales well with the number of parameters (unlike hypothesis tests). The uncertainty resulting from including/excluding AR(1) parameters is accounted for in the PPD. The TDAR inversion can also be used to evaluate the necessity of the AR(1) parameters; Table VI gives the proportion of samples with AR(1) parameters for both the scattering and reflection data. The results of the TDAR inversion are similar to the location tests and correctly differentiate the strongly and weakly correlated residuals at the various frequencies.

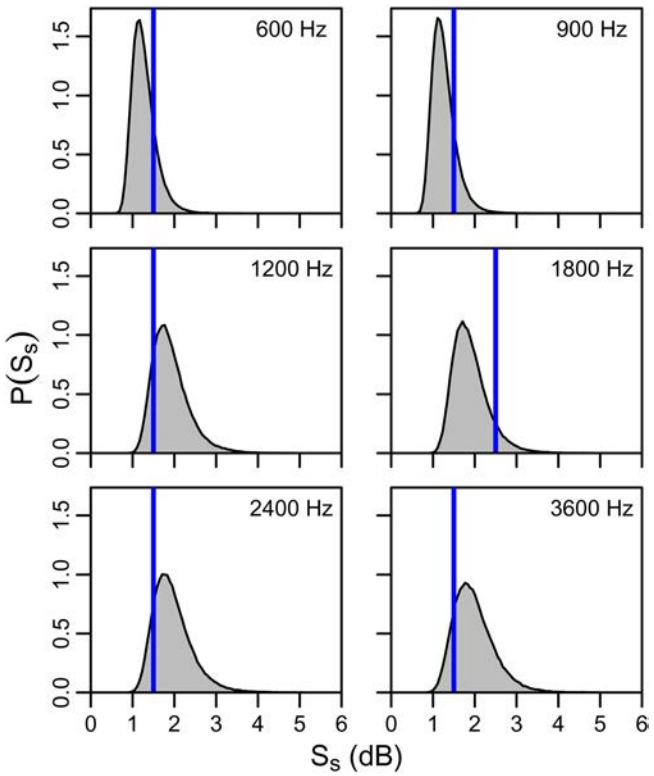

FIG. 11. (Color online) Marginal posterior distributions of the scattering data standard errors $\mathbf{S}_s$ for the joint inversion. Vertical lines indicate true values.

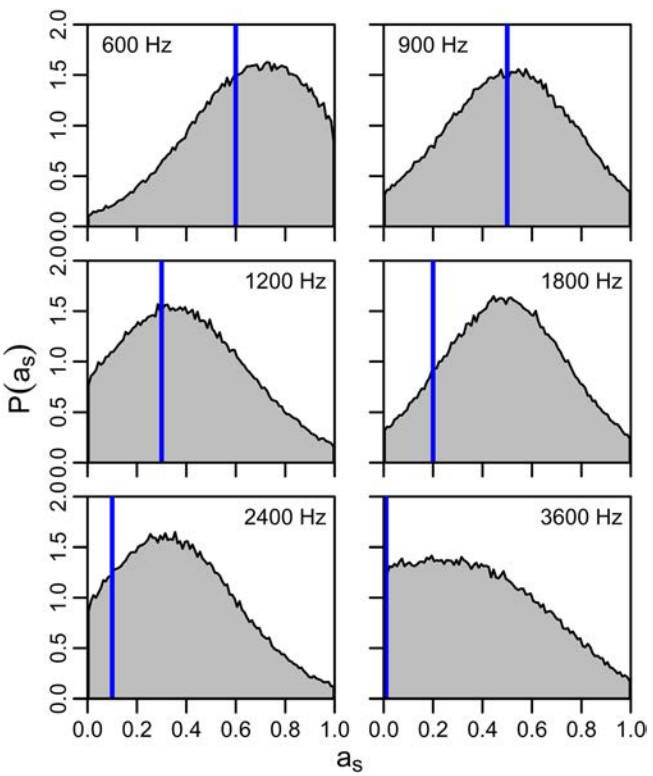

FIG. 12. (Color online) Marginal posterior distributions of the scattering data AR(1) parameters $\mathbf{a}_s$ for the joint inversion. Vertical lines indicate true values.

TABLE V. Location test results for AR(1) parameter means and p values for scattering (top) and reflection (bottom) errors from joint inversion.

Frequency (Hz)	600	900	1200	1800	2400	3600
Scattering means	0.621	0.518	0.408	0.491	0.381	0.404
p value	0.005	0.023	0.092	0.033	0.124	0.095
Frequency (Hz)	630	800	1000	1600	2500	4000
Reflection means	0.609	0.537	0.505	0.223	0.166	0.177
p value	0.000	0.000	0.000	0.036	0.108	0.088

VII. SUMMARY AND CONCLUSIONS

The rigorous estimation of *in situ* seabed scattering (roughness) parameters and their uncertainties from remote acoustic measurements is a problem of practical interest which has received little attention to date. This paper developed a Bayesian inversion approach to examine resolving a power-law representation of the 2D spatial roughness spectrum parameterized in terms of the spectral strength, exponent, and cut-off. The primary measurement of interest is the backscatter strength as a function of angle and frequency; however, since the scattering kernel also depends on the geoacoustic profile, the improvement in scattering spectral resolution from joint inversion of (simulated) backscatter and spherical-wave reflection-coefficient data was also examined and quantified. Basing initial inversion studies such as this on (realistic) simulations allows comparisons of results with the true model and control over error processes such that the information content of the physics of the acoustic measurements can be quantified. It is, of course, important to follow such studies with inversions of measured data, which represents future work.

The simulations considered here are based on observed scattering parameters and a realistic geoacoustic profile consisting of a large number of sediment layers ($\sim$100 layers over 6 m) with fine structure below the resolution limit of the data. An elastic half-space with compressional and shear properties representative of limestone comprised the basement. The number of sediment layers is unknown in the inversion and treated with a trans-D approach which samples over differing numbers of layers according to their support by the data and prior.

Realistic errors were added to the scattering and (unevenly-spaced) reflection data, including variances which changed with frequency (and near the critical angle for reflection data) and serial correlations which decreased with frequency such that only the low-frequency errors were significantly correlated. The error statistics were treated as unknown in the inversion and parameterized in terms of variances and AR(1) parameters. Given that error correlations were significant at only some frequencies, to avoid either over- or under-parameterizing the error model in the inversion, a new trans-D sampling approach was developed for the AR(1) parameters.

TABLE VI. Proportion of samples with the AR(1) parameter for scattering (top) and reflection (bottom) errors from TDAR inversion.

Frequency (Hz)	600	900	1200	1800	2400	3600
Scattering	0.9112	0.7858	0.5369	0.7469	0.5520	0.4474
Frequency (Hz)	630	800	1000	1600	2500	4000
Reflection	0.9995	1.0000	0.9997	0.4592	0.2426	0.2233

To treat a geoacoustic profile in which the number of parameters was not constant with depth (i.e., fluid sediment layers over an elastic basement) required developing a new trans-D partition prior distribution which is not based on a fictitious grid (the standard approach). This enhanced formulation also allows the explicit evaluation of the prior and posterior probabilities (rather than just relative probabilities). In addition, the prior used here includes empirical information on the relationship between compressional-wave velocity and density in sediments and limestone. This decreases the total volume of the parameter space without excluding plausible models, which is important in trans-D inversion where parsimony is based on the trade-off between data misfit and prior volume.

Three cases were considered: Scattering-only inversion, joint scattering and reflection inversion, and joint inversion with the trans-D auto-regressive error model. The ability of the inversions to resolve the model was evaluated using marginal posterior probability distributions and profiles. The resolution of the scattering parameters (particularly the spectral exponent) and geoacoustic parameters were improved by the introduction of the reflection data. The scattering-only inversion showed some sensitivity to the near surface geoacoustics; however, resolution decreased dramatically with depth. Both joint inversions resolved the geoacoustics at all depths. In the basement, the high shear-wave velocity was well resolved (better than compressional-wave velocity), highlighting the importance of including elasticity in an inversion when required by the data.

Auto-regressive models were found to effectively account for residual correlation in the scattering-only and joint inversion. However, including AR(1) parameters at all frequencies over-parameterized the error model and increased the variance of scattering parameters. The trans-D AR(1) scheme (i.e., the TDAR inversion) mitigated the loss of PPD resolution while accounting appropriately for the residual correlation at all frequencies.

The results in this paper indicate significant potential for Bayesian inversion of acoustic data to determine seabed scattering properties and uncertainties, particularly for joint inversion of scattering and reflection data.

ACKNOWLEDGMENTS

The authors gratefully acknowledge the support of an Office of Naval Research Grant (No. N00014-11-0213). The computational work was carried out on a parallel high-performance computing cluster operated by the authors at the University of Victoria funded by the Natural Sciences and Engineering Research Council of Canada and the Office of Naval Research.

[1]S. E. Dosso, "Quantifying uncertainty in geoacoustic inversion. I. A fast Gibbs sampler approach," J. Acoust. Soc. Am. **111**, 129–142 (2002).
[2]D. J. Battle, P. Gerstoft, W. S. Hodgkiss, W. A. Kuperman, and P. L. Nielsen, "Bayesian model selection applied to self-noise geoacoustic inversion," J. Acoust. Soc. Am. **116**, 2043–2056 (2004).

[3]Y. Jiang, N. R. Chapman, and H. A. DeFerrari, "Geoacoustic inversion of broadband data by matched beam processing," J. Acoust. Soc. Am. **119**, 3707–3716 (2006).
[4]C.-F. Huang, P. Gerstoft, and W. S. Hodgkiss, "Uncertainty analysis in matched-field geoacoustic inversions," J. Acoust. Soc. Am. **119**, 197–207 (2006).
[5]J. Dettmer, S. E. Dosso, and C. W. Holland, "Joint time/frequency-domain inversion of reflection data for seabed geoacoustic profiles," J. Acoust. Soc. Am. **123**, 1306–1317 (2008).
[6]D. Tollefsen and S. E. Dosso, "Bayesian geoacoustic inversion of ship noise on a horizontal array," J. Acoust. Soc. Am. **124**, 788–795 (2008).
[7]C. Yardim, P. Gerstoft, and W. S. Hodgkiss, "Tracking of geoacoustic parameters using Kalman and particle filters," J. Acoust. Soc. Am. **125**, 746–760 (2009).
[8]A. Gelman, J. B. Carlin, H. S. Stern, and D. B. Rubin, *Bayesian Data Analysis* (Chapman, New York, 2004), pp. 73–100.
[9]D. G. T. Denison, C. C. Holmes, B. K. Mallick, and A. F. M. Smith, *Bayesian Methods for Nonlinear Classification and Regression* (Wiley, New York, 2002), pp. 1–277.
[10]S. E. Dosso and P. Nielsen, "Quantifying uncertainty in Geoacoustic Inversion. II. Application to broadband, shallow-water data," J. Acoust. Soc. Am. **111**, 143–159 (2002).
[11]S. E. Dosso and C. W. Holland, "Geoacoustic uncertainties from viscoelastic inversion of seabed reflection data," IEEE J. Ocean. Eng. **31**, 657–671 (2006).
[12]P. J. Green, "Reversible jump Markov chain Monte Carlo computation and Bayesian model determination," Biometrika **82**, 711–732 (1995).
[13]P. J. Green, *Highly Structured Stochastic Systems*, Chap. Trans-dimensional Markov chain Monte Carlo, Oxford Statistical Science Series (Oxford University Press, Oxford, 2003), pp. 179–198.
[14]C. F. Mecklenbräuker, P. Gerstoft, J. F. Böhme, and P.-J. Chung, "Hypothesis testing for geoacoustic environmental models using likelihood ratio," J. Acoust. Soc. Am. **105**, 1738–1748 (1999).
[15]T. Jasa and N. Xiang, "Using nested sampling in the analysis of multi-rate sound energy decay in acoustically coupled rooms," AIP Conf. Proc. **803**, 189–196 (2005).
[16]J. Dettmer, S. E. Dosso, and C. W. Holland, "Model selection and Bayesian inference for high resolution seabed reflection inversion," J. Acoust. Soc. Am. **125**, 706–716 (2009).
[17]J. Dettmer, C. W. Holland, and S. E. Dosso, "Analyzing lateral seabed variability with Bayesian inference of seabed reflection inversions," J. Acoust. Soc. Am. **126**, 56–69 (2009).
[18]A. Malinverno, "Parsimonious Bayesian Markov chain Monte Carlo inversion in a non-linear geophysical problem," Geophys. J. Int. **151**, 675–688 (2002).
[19]M. Sambridge, K. Gallagher, A. Jackson, and P. Rickwood, "Trans-dimensional inverse problems, model comparison and the evidence," Geophys. J. Int. **167**, 528–542 (2006).
[20]N. P. Agostinetti and A. Malinverno, "Receiver function inversion by trans-dimensional Monte Carlo sampling," Geophys. J. Int. **181**, 858–872 (2010).
[21]T. Bodin and M. Sambridge, "Seismic tomography with the reversible jump algorithm," Geophys. J. Int. **178**, 1411–1436 (2009).
[22]J. Dettmer, S. E. Dosso, and C. W. Holland, "Trans-dimensional geoacoustic inversion," J. Acoust. Soc. Am. **128**, 3393–3405 (2010).
[23]J. Dettmer and S. E. Dosso, "Trans-dimensional matched-field geoacoustic inversion with hierarchical error models and interacting Markov chains," J. Acoust. Soc. Am. **132**, 2239–2250 (2012).
[24]J. Dettmer, S. Molnar, G. A. M. W. Steininger, S. E. Dosso, and J. F. Cassidy, "Trans-dimensional inversion of microtremor array dispersion data with hierarchical autoregressive error models," Geophys. J. Int. **188**, 719–734 (2011).
[25]C. W. Holland and J. Osler, "High-resolution geoacoustic inversion in shallow water: A joint time-and frequency-domain technique," J. Acoust. Soc. Am. **107**, 1263–1279 (2000).
[26]C. W. Holland, R. Hollett, and L. Troiano, "Measurement technique for bottom scattering in shallow water," J. Acoust. Soc. Am. **108**, 997–1011 (2000).
[27]J. Dettmer, S. E. Dosso, and C. W. Holland, "Uncertainty estimation in seismo-acoustic reflection travel-time inversion," J. Acoust. Soc. Am. **122**, 161–176 (2007).
[28]J. E. Moe and D. R. Jackson, "First-order perturbation solution for rough surface scattering cross section including the effects of gradients," J. Acoust. Soc. Am. **96**, 1748–1754 (1994).
[29]F. B. Jensen, W. A. Kuperman, M. B. Porter, and H. Schmidt, *Computational Ocean Acoustics, Series in Modern Acoustic and Signal Processing* (AIP Press, New York, 1993), pp. 1–64.
[30]R. Shumway and D. Stoffer, *Time Series Analysis and Its Applications* (Springer, New York, 2000), pp. 89–212.
[31]D. R. Jackson and M. D. Richardson, *High-Frequency Seafloor Acoustics*, 1st ed. (Springer, New York, 2007), pp. 178–200.
[32]J. Dettmer, S. E. Dosso, and C. W. Holland, "Full wave-field reflection coefficient inversion," J. Acoust. Soc. Am. **122**, 3327–3337 (2007).
[33]L. M. Brekhovskikh and O. A. Godin, *Acoustics of Layered Media II: Point Source and Bounded Beams*, Springer Series on Wave Phenomena, 1st ed. (Springer, New York, 1992), pp. 1–33.
[34]C. W. Holland, P. L. Nielsen, J. Dettmer, and S. E. Dosso, "Resolving meso-scale seabed variability using reflection measurements from an autonomous underwater vehicle," J. Acoust. Soc. Am. **131**, 1066–1078 (2012).
[35]E. L. Hamilton, "Geoacoustic modeling of the sea floor," J. Acoust. Soc. Am. **68**, 1313–1340 (1980).
[36]E. L. Hamilton and R. T. Bachman, "Sound velocity and related properties of marine sediments," J. Acoust. Soc. Am. **72**, 1891–1904 (1982).
[37]A. Jasra, D. A. Stephens, and C. Holmes, "Population-based reversible jump Markov chain Monte Carlo" Biometrika **94**, 787–807 (2007).
[38]D. J. Earl and M. W. Deem, "Parallel tempering: Theory, applications, and new perspectives," Phys. Chem. Chem. Phys. **7**, 3910–3916 (2005).
[39]S. E. Dosso, C. W. Holland, and M. Sambridge, "Parallel tempering for strongly nonlinear geoacoustic inversion," J. Acoust. Soc. Am. **132**, 3030–3040 (2012).